JOURNAL OF CATALYSIS **163,** 138–147 (1996)
ARTICLE NO. 0313

Kinetics and Deactivation of Sulfated Zirconia Catalysts for Butane Isomerization

Kevin B. Fogash, Robert B. Larson,[1] Martin R. González,[2] Jeffrey M. Kobe, and James A. Dumesic[3]

Department of Chemical Engineering, University of Wisconsin, 1415 Engineering Drive, Madison, Wisconsin 53706

Received March 11, 1996; revised June 3, 1996; accepted June 5, 1996

Reaction kinetics studies were conducted of *n*-butane and isobutane isomerization over sulfated zirconia at 423 K. The kinetic data can be described well by a rate expression based on a reversible, bimolecular surface reaction between two adsorbed *n*-C_4 species, probably through a C_8 intermediate, to produce one *i*-C_4 species, as well as surface reaction between two adsorbed *i*-C_4 species to produce one *n*-C_4 species. This reaction sequence also describes well the rates of C_4-disproportionation reactions to produce C_3 and C_5 species. The initial rate of catalyst deactivation is faster during *n*-butane isomerization than during isobutane isomerization, and the longer-term rate of deactivation during *n*-butane isomerization increases with the pressure of *n*-butane. The more rapid catalyst deactivation during *n*-butane isomerization may be related to the formation of *n*-C_4-diene species.

INTRODUCTION

Industrial isomerization reaction products are of particular importance due to the need for alkylates and reformulated gasoline. Sulfated zirconia is active for *n*-butane isomerization at low temperatures for which the formation of isobutane is thermodynamically favored (1). Various research groups (2–5) have suggested a bimolecular isomerization pathway involving a C_8 intermediate, while other groups (6) have suggested that the primary mode of butane isomerization involves the self-isomerization of the C_4 molecule through a cyclopropyl intermediate. In this paper, we have collected reaction kinetics data over a sulfated zirconia catalyst for the isomerization of *n*-butane to isobutane, as well as for the isomerization of isobutane to *n*-butane. These data are used to probe the nature of the dominant catalytic cycles, as well as the primary modes of deactivation, for this catalyst at temperatures near 423 K.

EXPERIMENTAL

The sulfated zirconia catalyst utilized in this study was provided by MEI (Flemington, NJ) in the form of a sulfated $Zr(OH)_4$ precursor, which was heated to 848 K in 1.5 h and maintained at this temperature for 2 h in 100 cm^3 (NTP)/min of dry O_2 per gram of precursor (where NTP designates 298 K and 1 atm). After activation, the catalyst was removed from the reactor and stored in a desiccator. This catalyst had a BET surface area of 98 m^2/g and a sulfur loading of 1.8 wt% (Galbraith Laboratories).

The details of the reaction kinetics measurements of *n*-butane isomerization are reported elsewhere (7). Typically, 500 mg of catalyst and 250 mg of quartz particles were loaded in a quartz reactor and dried for 1 h at 588 K in 65 cm^3 (NTP)/min of flowing, dry He (Liquid Carbonic). The *n*-butane reaction kinetics measurements were conducted at 423 K with various weight-hourly space-velocities (WHSV) of *n*-butane in the range of 2.0 to 20.2 h^{-1} (10 to 100% *n*-butane, AGA 99.5% purity instrument grade), with the balance consisting of dry He. The total flow rate was 65 cm^3 (NTP)/min. The major alkane impurities in the *n*-butane feed were isobutane and propane, for which the kinetics data were corrected. The *n*-butane contained C_4-olefins at a level of approximately 1200 ppm. Reaction kinetics measurements for isobutane isomerization were conducted at 423 K for values of WHSV from 2.0 to 20.2 h^{-1} (10 to 100% isobutane, AGA 99.5% purity instrument grade), with the balance consisting of dry He at a total flow rate of 65 cm^3 (NTP)/min. The major impurities in the isobutane feed were *n*-butane and propane, for which the kinetics data were corrected. The isobutane contained C_4-olefins at a level of approximately 400 ppm. The reaction products were analyzed with a Hewlett Packard 5890 gas chromatograph equipped with a 24-foot 5% DC-200 Chromosorb P-AW column, held at 323 K, with a flame ionization detector.

RESULTS

Figure 1 shows the rate of hydrocarbon production versus time on stream for isomerization of *n*-butane at 423 K at

[1] Current address: UOP, P.O. Box 163, Riverside, IL 60546-0163.
[2] Current address: Amoco Petroleum Products, 150 West Warrenville Road, Naperville, IL 60566-7011.
[3] To whom correspondence should be addressed.

0021-9517/96 $18.00

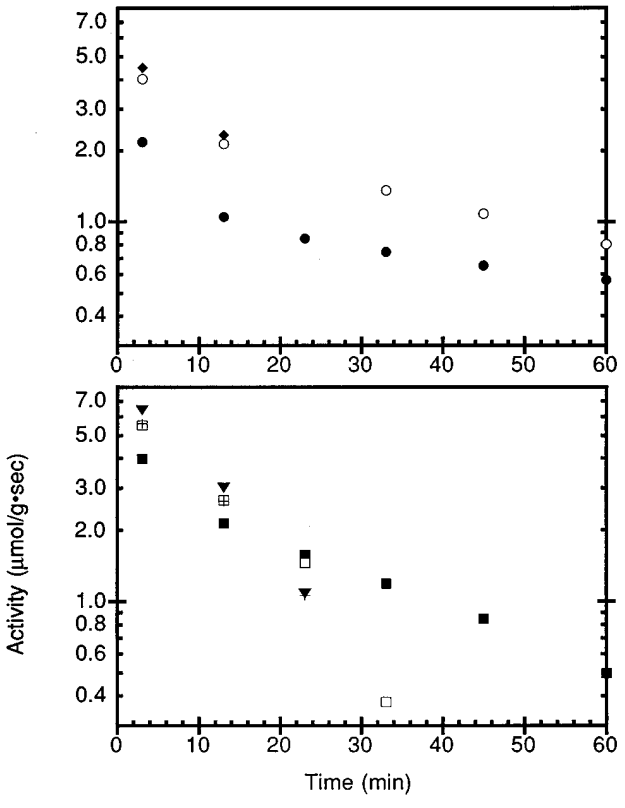

FIG. 1. Rates of hydrocarbon production (μmol/g · sec) versus time on stream for the isomerization of *n*-butane at 423 K for 10% (●), 23% (○), 28% (◆), 36% (■), 67% (□), 83% (▼), and 100% (+), *n*-butane in the feed.

various *n*-butane feed concentrations. The sulfated zirconia catalyst shows significant deactivation, and the rate of deactivation appears to be more rapid at higher concentrations of *n*-butane. For example, while the catalytic activity becomes very low after 2 h in 10% *n*-butane, the catalyst is essentially fully deactivated within 0.5 h in 100% *n*-butane.

Figure 2 displays the rate of isobutane production at 3 min on stream versus the percentage of *n*-butane in the feed stream, for the experiments presented in Fig. 1. These rates will be denoted as initial activities. The initial activity increases linearly for lower concentrations of *n*-butane in the feed, whereas the initial activity increases more gradually at higher concentrations. In addition, Fig. 2 shows the initial activities for the production of propane and isopentane for the various concentrations of *n*-butane in the feed. The only other species observed in any appreciable concentration was *n*-pentane (<20% of the isopentane level). Similar to the behavior of isobutane production, the initial rates of propane and isopentane production increase linearly for low concentrations of *n*-butane and increase more gradually at higher concentrations. Accordingly, the selectivity for isobutane production is essentially constant at 90–92% for the concentrations of *n*-butane employed in this study.

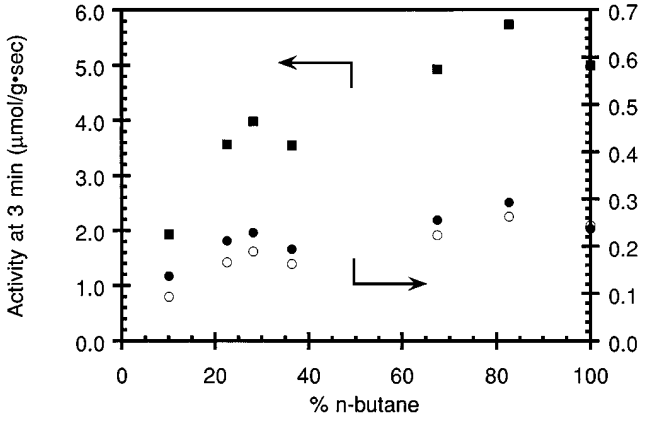

FIG. 2. Rates of hydrocarbon production at 3 min on stream versus percentage of *n*-butane in the feed. Left axis, isobutane (■); right axis, propane (●) and isopentane (○).

Figure 3 shows the rate of hydrocarbon production versus time on stream for isomerization of isobutane at 423 K for various isobutane feed concentrations. The sulfated zirconia catalyst deactivates slowly for isobutane isomerization in comparison to *n*-butane isomerization (Fig. 1). The rate of deactivation appears to be independent of isobutane concentration.

Figure 4 details the initial rate of *n*-butane production, as well as the initial rates of formation of propane and isopentane versus feed concentration of isobutane. These rates of *n*-butane, propane, and isopentane formation show a linear increase in rate at low isobutane concentrations and a more gradual increase at higher concentrations. The only other species observed in appreciable concentration was *n*-pentane (<20% of the isopentane level). The selectivity for *n*-butane production from isobutane is nearly constant at 65%. The initial rates of *n*-butane formation from isobutane in Fig. 4 are lower than for rates of isobutane formation

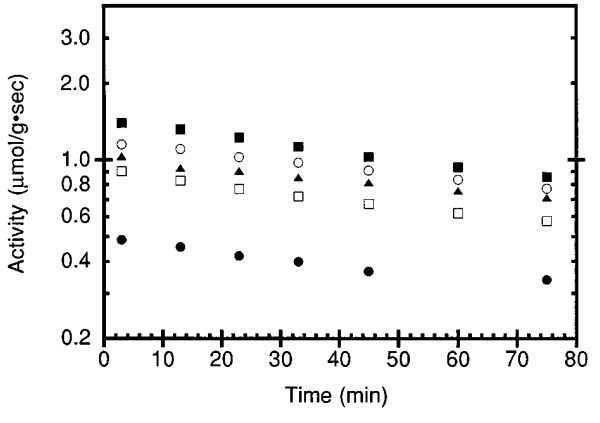

FIG. 3. Rates of hydrocarbon production (μmol/g · sec) versus time on stream for the isomerization of isobutane at 423 K for 10% (●), 25% (□), 53% (○), 77% (▲), and 100% (■), isobutane in the feed.

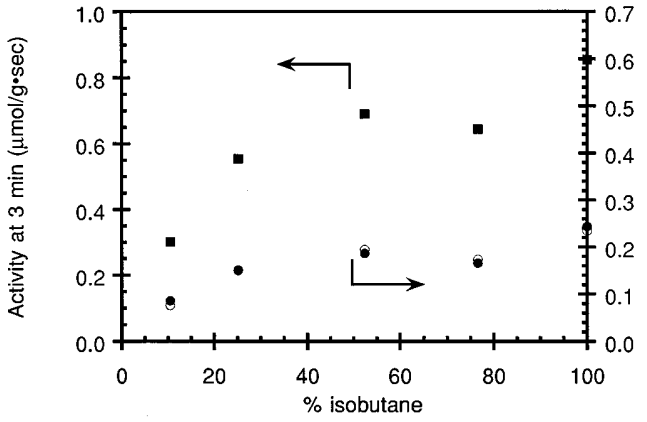

FIG. 4. Rates of hydrocarbon production at 3 min on stream versus percentage of isobutane in the feed. Left axis, *n*-butane (■); right axis, propane (●) and isopentane (○).

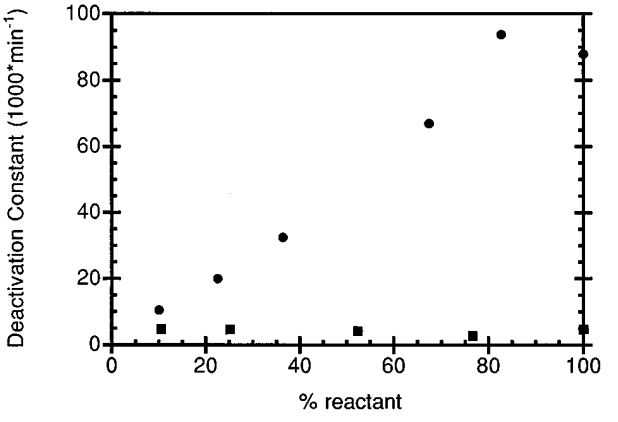

FIG. 6. Longer-term deactivation constants versus percentage of reactant in the feed stream for *n*-butane (●) and isobutane (■) isomerization.

from *n*-butane in Fig. 2. Importantly, the rate of catalyst deactivation appears to be significantly slower during the isomerization of isobutane to *n*-butane.

As shown elsewhere (8), significant regions of semi-log plots of catalytic activity versus time on stream are linear (Figs. 1 and 3) and can thus be described by a first-order deactivation relation,

$$R = R_0 \exp(-kt), \qquad [1]$$

where R_0 and R are the initial and subsequent rates of the isomerization reaction, and k is the rate constant of deactivation. Previously (8), we have divided the catalytic activity versus time into two regions: the initial activity region which encompasses the first 13 min of reaction and the longer-term region for data points beyond 13 min time on stream. Figure 5 shows the deactivation rate constants for the initial region versus percentage of reactant in the feed stream for isomerization of both *n*-butane and isobutane. The initial deactivation rate constant for *n*-butane isomerization is an order of magnitude higher than the initial deactivation rate constant for isobutane isomerization. These initial deactivation constants appear to be independent of the concentrations of *n*-butane or isobutane in the feed. Figure 6 shows the longer-term deactivation rate constants versus percentage of the reactant in the feed stream for isomerization of *n*-butane and isobutane. The deactivation rate constant for *n*-butane isomerization increases with *n*-butane concentration in the feed, whereas the deactivation rate constant for isobutane is fairly constant with respect to the amount of isobutane in the feed. Further, the elimination of the *n*-C_4-olefins (and possible *n*-C_4-dienes) in the feed (to levels <10 ppm) via an olefin trap (calcined H-mordenite held at 298 K) reduced the longer-term deactivation constant for a pure *n*-butane feed from ca. 0.1 min^{-1} to ca. 0.007 min^{-1}. Similar behavior has been seen by Liu *et al.* (9) over sulfated zirconia using an upstream Pt/SiO_2 bed with a co-feed of hydrogen.

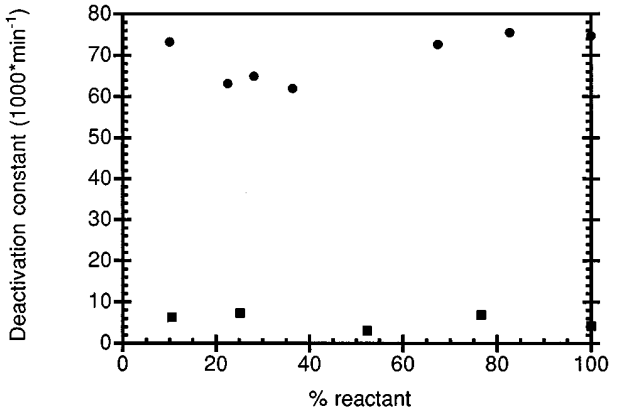

FIG. 5. Deactivation constants for the initial region versus percentage of reactant in the feed stream for *n*-butane (●) and isobutane (■) isomerization.

DISCUSSION

The isomerization of *n*-butane can be described in terms of intermolecular and/or intramolecular processes. Intramolecular isomerization of *n*-butane may take place via a cyclopropyl intermediate, involving formation of a primary carbenium ion. For intermolecular isomerization, *n*-butane interacts with another molecule to form a C_8 intermediate, which undergoes subsequent isomerization and β-scission to form isobutane.

Garin *et al.* (6) proposed that C_4 isomerization occurred via an intramolecular process over sulfated zirconia at 523 K in the presence of hydrogen. In this monomolecular process, the adsorbed C_4 species would self-isomerize via a cyclopropane intermediate to form an adsorbed isobutane species. However, Adeeva *et al.* (3) found that intramolecular rearrangement of the double ^{13}C-labeled *n*-butane,

$^{13}CH_3$–CH_2–CH_2–$^{13}CH_3$, resulted in $^{13}CH_3$–CH_2–$^{13}CH_2$–CH_3. Brouwer (10) found that in liquid superacids the isomerization of $^{13}CH_3$–CH_2–CH_2–CH_3 to CH_3–$^{13}CH_2$–CH_2–CH_3 is fast in comparison to the formation of isobutane. Further, Boronat *et al*. (11) suggested that the formation of isobutane and a scrambled *n*-butane follow different reaction pathways.

Sachtler and co-workers (2, 3) used isotopic analysis of *n*-butane isomerization over sulfated zirconia as well as Fe- and Mn-promoted sulfated zirconia at low temperatures to show that butane isomerization was an intermolecular process, and these authors suggested the presence of a C_8 intermediate. Gates and co-workers (4, 5, 12) also suggested an intermolecular pathway for *n*-butane and isobutane isomerization over Fe- and Mn-modified sulfated zirconia. Their observation of equimolar amounts of disproportionation products, C_3 and C_5 species, suggested the presence of a C_8 intermediate, as Bearez *et al*. (13) proposed for *n*-butane isomerization over H-mordenite. Accordingly, the C_8 species can function as an intermediate for both isomerization and disproportionation reactions as suggested by Asuquo *et al*. (14) over H-mordenite. Recently, Liu *et al*. (9) proposed a bimolecular mechanism for butane isomerization even in the presence of hydrogen. Furthermore, Tábora *et al*. (15) suggested a bimolecular mechanism in which β-scission of the C_8 intermediate results in a butyl and an isobutyl species.

As observed by other investigators (4, 12, 16), we have found that the rates of production of C_3 and C_5 are approximately equal, suggesting that the disproportionation of a C_8 species is responsible for these reaction products. If C_4 isomerization occurs via an intramolecular process and disproportionation occurs via an intermolecular process, then the rates of these processes would show different variations with respect to feed concentration. Yet, the rates of these processes are independent of feed concentration, such that the selectivity for isomerization is independent of the feed concentration for the isomerization of both *n*-butane and isobutane. Thus, the similar trends in the production rates of the isomerized species and the disproportionation products strongly suggest that the isomerization and disproportionation pathways occur through intermolecular processes involving C_8 intermediates.

Possible routes for *n*-C_4 isomerization via C_8 intermediates are shown schematically in Fig. 7. The C_8 intermediate formed from two *n*-butane surface species is most likely a secondary carbenium ion (3,4-dimethylhexane, species I) which can form a tertiary carbenium ion (2,4-dimethylhexane, species II) via nonbranching methyl and hydride shifts. Species II can undergo β-scission to form a

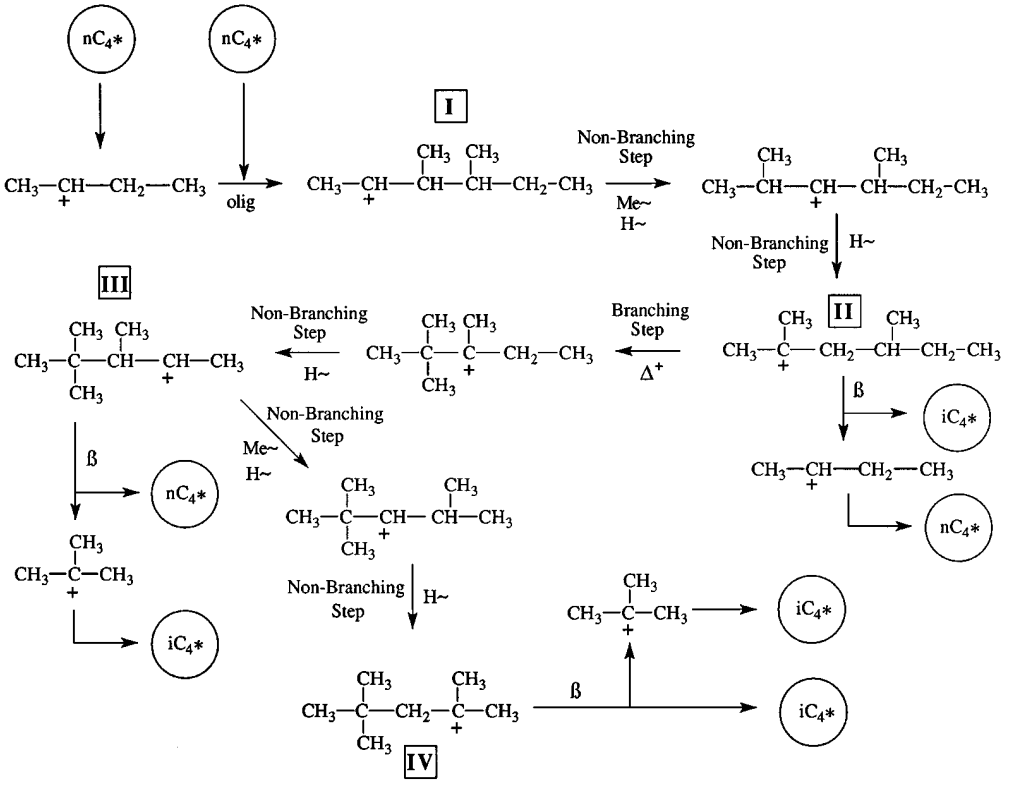

FIG. 7. Possible pathways for C_4 isomerization via C_8 intermediates. olig, oligomerization; β, β-scission; Δ^+, cyclopropyl ring formation; H~, hydride shift; Me~, methyl shift; *n*C_4* and *i*C_4* refer to surface species.

secondary *n*-butyl carbenium ion and an isobutyl species. Alternatively, species II can form a secondary carbenium ion (2,2,3-trimethylpentane, species III) via a branching rearrangement involving cyclopropyl ring formation and hydride shift. Species III can then undergo β-scission to form a tertiary isobutyl carbenium ion and an *n*-butyl species. In addition, species III can form a tertiary carbenium ion (2,2,4-trimethylpentane, species IV) through nonbranching methyl and hydride shifts. Finally, β-scission of species IV results in a tertiary isobutyl carbenium ion and an isobutyl species.

Brouwer (10) proposed that trimethylpentane cations can rapidly equilibrate with all other trimethylpentane cations in liquid superacids, and the preferred cleavage pathway is through the 2,2,4-trimethylpentane cation to form a tertiary isobutane cation and isobutylene. Furthermore, nonbranching rearrangements are faster than branching rearrangements. Thus, for the reaction of two *n*-butane species, β-scission of the 2,2,4-trimethylpentane cation (species IV) resulting in a tertiary isobutyl carbenium ion and an isobutyl species is a possible pathway for *n*-butane isomerization, as is β-scission of the 2,2,3-trimethylpentane cation (species III) to form a tertiary isobutyl carbenium ion and an *n*-butyl species. Thus, if β-scission of the 2,4-dimethylhexane cation (species II) to form a secondary *n*-butyl carbenium ion and an isobutyl species is faster than the branching rearrangement of species II, then β-scission of the 2,4-dimethylhexane cation is a viable pathway for *n*-butane isomerization.

More importantly, the reaction of two isobutane species during isobutane isomerization will form the 2,2,4-trimethylpentane cation (species IV). This C_8 intermediate must proceed through species II and then species I to form two *n*-butane species. However, the 3,4-dimethylhexane cation (species I) is less stable than the 2,4-dimethylhexane cation (species II). Thus, β-scission of the 2,4-dimethylhexane cation to form a secondary *n*-butyl carbenium ion and an isobutyl species is the more probable pathway for isobutane isomerization than β-scission of 3,4-dimethylhexane to form a secondary *n*-butyl carbenium ion and an *n*-butyl species. However, both pathways depend on the branching rearrangement step from species III to species II, which is slow. Another pathway, as proposed by Bearez *et al*. (17) for isobutane isomerization over H-mordenite, involves cleavage of the 2,2,3-trimethylpentane cation (species III) to form a tertiary isobutyl carbenium ion and an *n*-butyl species. Thus, if β-scission of the 2,2,3-trimethylpentane cation (species III) to form a tertiary isobutyl carbenium ion and an *n*-butyl species is faster than the branching rearrangement of species III, which is likely as a tertiary carbenium ion is more stable than a secondary carbenium ion, then β-scission of the 2,2,3-trimethylpentane cation is a viable pathway for isobutane isomerization.

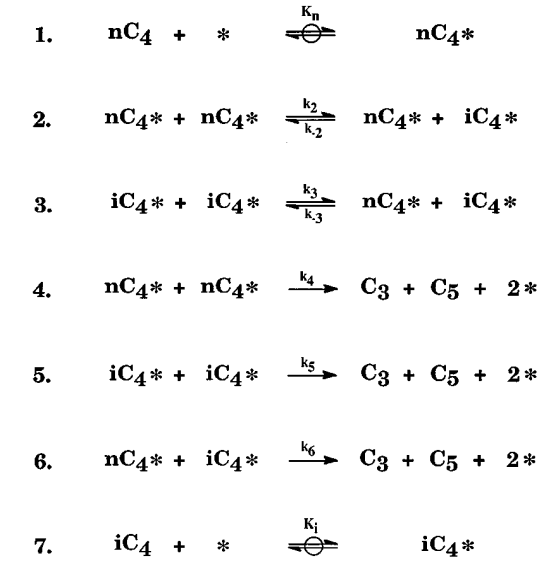

FIG. 8. Proposed catalytic cycles for isomerization and disproportionation of butane over sulfated zirconia.

Figure 8 shows one possible scheme for the isomerization and disproportionation of butane over sulfated zirconia, with the corresponding equilibrium constants (K_n, K_i) and rate constants (k_2, k_{-2}, k_3, k_{-3}, k_4, k_5, k_6) shown for each step. Irreversible steps are designated by single arrows, reversible steps are shown as forward and reverse arrows, and quasi-equilibrated steps are given by forward and reverse arrows connected by a circle. Step 1 involves the quasi-equilibrated adsorption/desorption of *n*-butane on the surface. Step 2 is the reversible reaction of two *n*-butane surface species to form an adsorbed isobutane species and an adsorbed *n*-butane species. Step 3 is the reversible reaction of two adsorbed isobutane species to form an adsorbed *n*-butane species and an adsorbed isobutane species. Steps 4–6 produce C_3 and C_5 species from the C_8 intermediate. Steps 4–6 are irreversible and represent combinations of individual steps involving the formation of the C_8 intermediate and subsequent disproportionation and desorption. Step 7 is the quasi-equilibrated adsorption/desorption of the adsorbed isobutane species.

The observed reaction kinetics can be effectively described by these catalytic cycles using Hougen–Watson rate equations:

$$r_{\text{isomerization}} = \frac{k_2 K_n^2 P_n^2 - k_{-2} K_n K_i P_n P_i - k_3 K_i^2 P_i^2 + k_{-3} K_n K_i P_n P_i}{(1 + K_n P_n + K_i P_i)^2} \quad [2]$$

$$r_{\text{disproportionation}} = \frac{k_4 K_n^2 P_n^2 + k_5 K_i^2 P_i^2 + k_6 K_n K_i P_n P_i}{(1 + K_n P_n + K_i P_i)^2}. \quad [3]$$

These relations are derived by first writing the following

competitive Langmuir isotherms for the adsorption of n-C_4 and i-C_4 species (θ_n and θ_i, respectively);

$$\theta_n = \frac{K_n P_n}{(1 + K_n P_n + K_i P_i)} \quad [4]$$

$$\theta_i = \frac{K_i P_i}{(1 + K_n P_n + K_i P_i)}, \quad [5]$$

and then writing the following expressions for the rates of isomerization and disproportionation:

$$r_{\text{isomerization}} = k_2\theta_n\theta_n - k_{-2}\theta_n\theta_i - k_3\theta_i\theta_i + k_{-3}\theta_n\theta_i \quad [6]$$

$$r_{\text{disproportionation}} = k_4\theta_n\theta_n + k_5\theta_i\theta_i + k_6\theta_n\theta_i. \quad [7]$$

The aforementioned model for isomerization (Eq. [2]) involving reaction of either two n-butane species or two isobutane species to form a single isobutane and a single n-butane species shall be denoted as model 1. Alternative models for n-butane isomerization can be derived in a manner similar to that in model 1, and these models are presented in Table 1 with their corresponding rate expressions as well as the necessary thermodynamic constraints for the parameters. Model 2 involves reaction of two n-butane species to form two isobutane species. Model 3 involves reaction of two n-butane species to form two isobutane species and reaction of two isobutane species to form a single n-butane and a single isobutane species. Model 4 involves reaction of two n-butane species to form a single isobutane and a single n-butane species and reaction of two isobutane species to form two n-butane species.

TABLE 2

Kinetic Parameters for Butane Isomerization

	Rate constant (μmol/g·sec)	Estimated error (μmol/g·sec)		Equilibrium constant	Estimated error
k_2	6.39	0.64	K_n	17.0	5.0
k_{-2}	5.06	0.50	K_i	12.6	10.9
k_3	0.87	0.68			
k_{-3}	1.10	0.86			
k_4	0.29	0.18	K_{eq}	1.7[a]	
k_5	0.25	0.21			
k_6	0.58	2.22			

[a] Pines, H., Kvetinskas, B., Kassel, L. S., and Ipatieff, V. N., *J. Am. Chem. Soc.* **67**, 631 (1945). The standard state is 1 atm and 423 K, the reaction temperature.

The rates of isomerization and disproportionation measured for the various feeds of n-butane and isobutane employed in this study can be described by Eqs. [2] and [3] in terms of seven parameters: K_n, K_i, k_2, k_{-3}, k_4, k_5, and k_6. The values of the reverse rate constant of step 2 and the forward rate constant of step 3 are determined from the isomerization equilibrium constant at 423 K. Table 2 shows the values of the kinetic parameters resulting from a nonlinear, least-squares fit of the kinetic data. A method described by Box *et al.* (18) was used to estimate 95% confidence levels for the parameters.

TABLE 1

Butane Isomerization Models

Model	Mechanism	Isomerization rate expression	Thermodynamic constraints
1	$nC_4* + nC_4* \underset{k_{-2}}{\overset{k_2}{\rightleftharpoons}} nC_4* + iC_4*$ $iC_4* + iC_4* \underset{k_{-3}}{\overset{k_3}{\rightleftharpoons}} nC_4* + iC_4*$	$r = \frac{k_2K_n^2P_n^2 - k_{-2}K_nK_iP_nP_i - k_3K_i^2P_i^2 + k_{-3}K_nK_iP_nP_i}{(1 + K_nP_n + K_iP_i)^2}$	$k_{-2} = \frac{K_nk_2}{K_iK_{eq}}$ $k_3 = \frac{K_nk_{-3}}{K_iK_{eq}}$
2	$nC_4* + nC_4* \underset{k_{-2}}{\overset{k_2}{\rightleftharpoons}} iC_4* + iC_4*$	$r = \frac{2k_2K_n^2P_n^2 - 2k_{-2}K_i^2P_i^2}{(1 + K_nP_n + K_iP_i)^2}$	$k_{-2} = \frac{K_n^2k_2}{K_i^2K_{eq}^2}$
3	$nC_4* + nC_4* \underset{k_{-2}}{\overset{k_2}{\rightleftharpoons}} iC_4* + iC_4*$ $iC_4* + iC_4* \underset{k_{-3}}{\overset{k_3}{\rightleftharpoons}} nC_4* + iC_4*$	$r = \frac{2k_2K_n^2P_n^2 - 2k_{-2}K_i^2P_i^2 - k_3K_i^2P_i^2 + k_{-3}K_nK_iP_nP_i}{(1 + K_nP_n + K_iP_i)^2}$	$k_{-2} = \frac{K_n^2k_2}{K_i^2K_{eq}^2}$ $k_3 = \frac{K_nk_{-3}}{K_iK_{eq}}$
4	$nC_4* + nC_4* \underset{k_{-2}}{\overset{k_2}{\rightleftharpoons}} nC_4* + iC_4*$ $iC_4* + iC_4* \underset{k_{-3}}{\overset{k_3}{\rightleftharpoons}} nC_4* + nC_4*$	$r = \frac{k_2K_n^2P_n^2 - k_{-2}K_nK_iP_nP_i - 2k_3K_i^2P_i^2 + 2k_{-3}K_n^2P_n^2}{(1 + K_nP_n + K_iP_i)^2}$	$k_{-2} = \frac{K_nk_2}{K_iK_{eq}}$ $k_3 = \frac{K_n^2k_{-3}}{K_i^2K_{eq}^2}$

Note. All models have quasi-equilibrated n-butane and isobutane adsorption steps: $nC_4 + * \overset{K_n}{\rightleftharpoons} nC_4*$ $iC_4 + * \overset{K_i}{\rightleftharpoons} iC_4*$.

TABLE 3

Comparison of Observed and Predicted Rates of Butane Isomerization at 423 K

% *n*-Butane in outlet stream at 3 min	% Isobutane in outlet stream at 3 min	Observed rate of isomerization (μmol/g·sec)	Observed rate of disproportionation (μmol/g·sec)	Predicted rate of isomerization (μmol/g·sec)	Predicted rate of disproportionation (μmol/g·sec)	Deviation^2 (μmol/g·sec)^2
8.33	1.86	1.93	0.12	2.00	0.11	5.42E−03[a]
19.1	3.76	3.57	0.19	3.37	0.18	5.15E−02[a]
24.2	4.28	3.99	0.21	3.73	0.20	8.68E−02[a]
32.9	3.74	3.55	0.18	4.14	0.21	4.68E−01[a]
62.5	5.35	4.93	0.24	4.95	0.24	1.23E−03[a]
77.3	6.00	5.74	0.28	5.18	0.25	3.97E−01[a]
95.3	5.37	5.00	0.24	5.35	0.26	1.43E−01[a]
0.44	10.2	−0.30	0.08	−0.31	0.08	1.39E−03[b]
0.70	24.7	−0.55	0.15	−0.53	0.14	8.04E−03[b]
1.00	51.7	−0.69	0.19	−0.69	0.19	1.08E−03[b]
1.07	76.0	−0.64	0.17	−0.74	0.20	2.17E−01[b]
1.32	99.2	−0.85	0.24	−0.77	0.21	1.37E−01[b]
					Sum of squares	1.52

[a] Deviation^2 = (deviation of the predicted isomerization rate)^2 + 100 × (deviation of the predicted disproportionation rate)^2.
[b] Deviation^2 = 10 × (deviation of the predicted isomerization rate)^2 + 100 × (deviation of the predicted disproportionation rate)^2.

The isomerization rate constant for reaction of two *n*-butane species is ca. 7 times faster than the rate constant for reaction of two isobutane species. Further, the rate of reaction between two *n*-butane molecules to form C_3 and C_5 species is similar to the disproportionation rate of two isobutane molecules. The rate of reaction of *n*-butane with isobutane to form C_3 and C_5 species appears to be rather fast; however, the confidence interval for k_6 is large because this parameter has a small effect on reaction kinetic data collected under the conditions of our study, which suggests that this pathway may not be important under our experimental conditions. Finally, the adsorption equilibrium constants for both *n*-butane, K_n, and isobutane, K_i, are approximately equal.

Table 3 presents values of the experimental and the predicted rates of butane isomerization and disproportionation using a plug-flow reactor model. Positive values of the isomerization rate represent production of isobutane. The experimental disproportionation rate is the average rate of production of C_3 and C_5 species. It can be seen in this table that the agreement between the experimental and predicted rates is very good for isomerization as well as for disproportionation with the sum of squares of the deviation of the predicted values and the experimental values equal to 1.52 (μmol/g·sec)^2, where the disproportionation rates have been weighted by a factor of 100 and the rates of isobutane isomerization have been weighted by a factor of 10.

The trends in the rates versus outlet concentration at 3 min time on stream are shown in Figs. 9 and 10 for the conversions of *n*-butane and isobutane, respectively. The predicted rates are given by the curves. In all cases, the trends in the rates of isomerization and disproportionation for both the *n*-butane and the isobutane reactions were accurately described by our catalytic cycles and kinetic parameters.

When model 2 is used to fit the data set, the sum of squares is equal to 2.01 (μmol/g·sec)^2, which is larger than the sum of squares for model 1. Model 3 reverted to model 2 in fitting the data set, with a sum of squares of 2.01 (μmol/g·sec)^2. Model 4 fit the data well with a sum of squares of 1.52 (μmol/g·sec)^2.

It is interesting to extend our kinetic analysis to the work of Gates and co-workers (5) involving C_4 isomerization over a promoted sulfated zirconia catalyst at 333 K. Zarkalis *et al.* (5) utilized a rate expression based on a reversible second-order (intermolecular) surface reaction between two adsorbed *n*-butane species to form two adsorbed isobutane

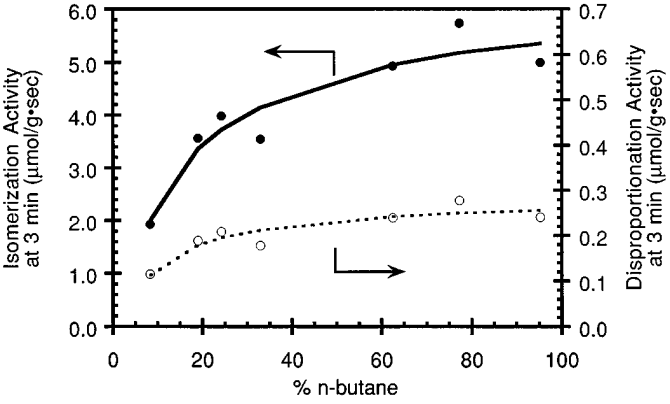

FIG. 9. Experimental (●) and predicted (—) rates of isomerization (left axis) and experimental (○) and predicted (- - -) rates of disproportionation (right axis) versus percentage of *n*-butane in the outlet stream at 3 min.

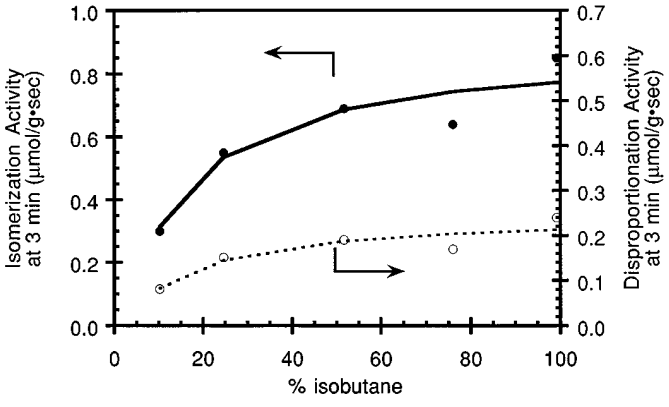

FIG. 10. Experimental (●) and predicted (—) rates of isomerization (left axis) and experimental (○) and predicted (- - -) rates of disproportionation (right axis) versus percentage of isobutane in the outlet stream at 3 min.

species, which can be represented by model 2, to fit their kinetic data, as shown in Table 4. For comparison, we have attempted to describe, using a well-mixed reactor, the kinetic data collected by Gates and co-workers (5) in terms of our rate expression (model 1), based on intermolecular surface reaction between two adsorbed *n*-butane species to form adsorbed isobutane and adsorbed *n*-butane, as well as reaction between two adsorbed isobutane species to form adsorbed isobutane and adsorbed *n*-butane. It can be seen in Table 4 that the sum of squares of the deviation of the predicted values and the experimental values is 0.198 $(\mu\text{mol/g}\cdot\text{sec})^2$, where the rates of isobutane isomerization and the smaller rates of *n*-butane isomerization have been weighted by a factor of 10. In comparison, Zarkalis *et al.* (5) reported a sum of the squares of 2.3 $(\mu\text{mol/g}\cdot\text{sec})^2$ for their preferred second order rate expression. For our model 2, we obtained a sum of the squares of 0.382 $(\mu\text{mol/g}\cdot\text{sec})^2$ utilizing our weighting scheme. The values for the adsorption equilibrium constants given by our fit of the data using Eq. [2] are similar to the values provided by Zarkalis *et al.* (5) for their second order rate expression.

It is apparent from Table 4 that the rate expression of Eq. [2], representing the surface reaction of two C_4 species to form one isomerized C_4 species, more accurately describes the rate of C_4 isomerization than a rate expression based on surface reaction of two C_4 species to form two isomerized C_4 species. Further, the rate expression accurately predicts the direction of isomerization, especially for small rates of isomerization (<0.1 $\mu\text{mol/g}\cdot\text{sec}$).

The rate expression of Eq. [2] is a four-parameter model, whereas the second order rate expression of Zarkalis *et al.* (5) can be represented as a three-parameter model. Thus the second-order model of Zarkalis *et al.* (5) can be considered to be subset of the rate expression in Eq. [2], where k_2 and k_3 have been combined into a single parameter. For nested models, an analysis of the extra sum of squares

TABLE 4

Comparison of Observed and Predicted Rates of Butane Isomerization at 333 K[a]

Observed rate (μmol/g·sec)	Model 2 predicted rate (μmol/g·sec)	Model 1 predicted rate (μmol/g·sec)	Model 2 deviation^2 $(\mu\text{mol/g}\cdot\text{sec})^2$	Model 1 deviation^2 $(\mu\text{mol/g}\cdot\text{sec})^2$
1.82	1.56	1.57	6.99E−02	6.1E−02
0.973	1.17	1.14	3.78E−02	2.8E−02
2.01	1.91	1.98	1.07E−02	9.3E−04
2.06	2.00	2.09	4.03E−03	7.2E−04
2.07	2.05	2.15	4.67E−04	6.2E−03
1.36	1.46	1.35	9.33E−03	3.0E−05
0.928	1.03	0.917	1.03E−02	1.2E−04
0.503	0.612	0.527	1.18E−01[b]	5.6E−03[b]
−0.213	−0.169	−0.216	1.93E−02[b]	7.1E−05[b]
−0.241	−0.220	−0.251	4.37E−03[b]	1.1E−03[b]
−0.261	−0.242	−0.265	3.58E−03[b]	1.7E−04[b]
−0.212	−0.169	−0.216	1.85E−02[b]	1.3E−04[b]
0.047	0.038	0.033	8.56E−04[b]	1.9E−03[b]
−0.012	−0.008	−0.007	1.56E−04[b]	2.3E−04[b]
−0.036	−0.037	−0.033	9.14E−06[b]	7.1E−05[b]
−0.15	−0.078	−0.071	5.22E−02[b]	6.2E−02[b]
−0.173	−0.127	−0.120	2.11E−02[b]	2.8E−02[b]
0.019	0.007	0.006	1.46E−03[b]	1.7E−03[b]
		Sum of squares of the deviations	0.382	0.198

[a] Data from Zarkalis *et al.* (1994).
[b] Data sets where the deviation^2 has been weighted by a factor of 10.

due to the extra parameter between the full model and the partial model can be performed to determine which nested model adequately fits the data with the minimum number of parameters (19). Briefly, the partial model is accepted if the calculated value of the mean square ratio is less than the tabulated F distribution for the desired confidence level. For one degree of freedom for the extra parameter (ν_e) and 14 degrees of freedom for the full model (ν_f), the tabulated F value at a 95% confidence level is 4.60. The calculated value of the mean square ratio is 13.01, from the sum of squares: $S_{full} = 0.198$ $(\mu mol/g \cdot sec)^2$ and $S_{partial} = 0.382$ $(\mu mol/g \cdot sec)^2$, where the mean square ratio is $(S_{extra}/\nu_e)/(S_{full}/\nu_f)$ with $S_{extra} = S_{partial} - S_{full}$. Because $13.01 > 4.60$, we suggest that the rate expression of Eq. [2], representing the surface reaction of two C_4 species to form one isomerized C_4 species, is preferred over the second order model based on surface reaction of two C_4 species to form two isomerized C_4 species.

For completeness, we also used models 3 and 4 to fit the kinetic data collected by Gates and co-workers (5). Model 3 fit the data well with a sum of the squares of 0.198 $(\mu mol/g \cdot sec)^2$ utilizing our weighting scheme. Model 4 reverted to model 2, with a sum of squares of 0.382 $(\mu mol/g \cdot sec)^2$.

Among the various models presented in Table 1, we find that model 1, which represents the reaction of either two *n*-butane species or two isobutane species to form a single isobutane and a single *n*-butane species, fits both our data and the data from Gates and co-workers (5). Model 2 also fits both data sets, but not to the same degree as model 1. Model 3 reverts to model 2 for our data set, but fits the data from Gates and co-workers (5) to the same degree as model 1. Model 4 reverts to model 2 for the data set from Gates and co-workers (5), but fits our data to the same degree as model 1.

The fitting of our data for *n*-butane isomerization to model 1 suggests that β-scission occurs for the 2,4-dimethylhexane cation (species II, Fig. 7) or the 2,2,3-trimethylpentane cation (species III, Fig. 7). For isobutane isomerization, β-scission of the 2,4-dimethylhexane cation (species II, Fig. 7) to form a secondary *n*-butyl carbenium ion and an isobutyl species is the more probable pathway for reaction than β-scission of 3,4-dimethylhexane (species I, Fig. 7) to form a secondary *n*-butyl carbenium ion and an *n*-butyl species. Alternatively, Bearez *et al.* (17) proposed that cleavage of the C_8 intermediate occurs via the 2,2,3-trimethylpentane cation (species III, Fig. 7) to form a tertiary isobutyl carbenium ion and an *n*-butyl species for isobutane isomerization over H-mordenite. In either case, the reaction of two isobutane species via a C_8 intermediate forms one *n*-C_4 species, which is in agreement with our rate expression.

Recently, Liu *et al.* (9) have proposed an intermolecular mechanism for *n*-butane isomerization utilizing the pressure of the olefin (C_4H_8), where the pressure of the olefin is replaced by the equilibrium expression for the olefin involving the paraffin (C_4H_{10}) and H_2. This model does not fit the data from Zarkalis *et al.* (5) as well as the second order model (model 2). Furthermore, we do not observe significant olefin concentrations (i.e., greater than 1 ppm) in the effluent stream during our experiments when an olefin trap is used upstream of the catalyst bed. Thus, it appears that equilibration between gaseous paraffins and olefins does not occur over our catalyst system (that does not contain Pt) in the absence of hydrogen. However, this lack of equilibration between gaseous species does not discount the promotional effect of the addition of olefins, as seen by Tábora *et al.* (15) for butane isomerization over sulfated zirconia. Specifically, the adsorbed *n*-butane surface species (step 1, Fig. 8) can be olefinic in nature, and thus addition of olefins in the feed stream could increase the surface concentration of *n*-C_4* species which would increase the isomerization rate (step 2, Fig. 8).

Sachtler and co-workers (2, 3) observed that *n*-butane reactants each containing two ^{13}C atoms formed isobutane species containing a binomial distribution of ^{13}C atoms; however, the remaining *n*-butane species reached the binomial distribution of ^{13}C atoms more slowly. This behavior can be reconciled with model 1 if nonbranching rearrangements of species III are more rapid than the β-scission step to give *n*-butyl species and a tertiary carbenium ion and also more rapid than the branching step to give species II.

It can be seen in Table 2 that the rate constant for the production of *n*-butane isomerization (k_2) is ca. 7 times larger than the rate constant for the isomerization of isobutane (k_3). Further, the selectivity for *n*-butane isomerization is 92%, while the selectivity for isobutane isomerization was ca. 65%. Also, the equilibrium constants for *n*-butane and isobutane adsorption, 17.0 and 12.6, respectfully, are very similar. This latter result is consistent with our microcalorimetric work (20) in which the coverages and heats of adsorption were similar for *n*-butane and isobutane adsorption on sulfated zirconia. Thus, the differences in the selectivities and the rates of isomerizations between *n*-butane and isobutane are not related to differences in adsorption or desorption of the C_4 species. Rather, it appears that the formation of the C_8 intermediate is favored when two *n*-butyl species react, as opposed to reaction between two isobutyl species. Most likely, the *n*-butyl species offers less steric hindrance or more C–H bonds that may react to form the C_8 intermediates. Alternatively, the preferred cleavage pathway for the C_8 intermediate formed from two isobutane species may be to reform the two isobutyl reactants, as suggested by Brouwer (10), thereby explaining the lower rate of isobutane isomerization to *n*-butane.

It can be seen in Fig. 5 that the initial rate of deactivation is independent of the pressure of the reactant, and it is an order of magnitude faster for *n*-butane isomerization

than for isobutane isomerization. Moreover, as shown in Fig. 6, the longer-term rate of deactivation during *n*-butane isomerization depends upon the pressure of the *n*-butane in the feed, while the rate of deactivation during isobutane isomerization remains slow at all isobutane pressures. Thus, we conclude that the primary cause of catalyst deactivation under our experimental conditions is related to the presence of *n*-butane.

The most important modes of deactivation for sulfated zirconia catalysts have been suggested to be reduction of surface sulfate species (21, 22) and formation of carbonaceous deposits on the active sites (4, 23–25). We note that *n*-butane is able to undergo multiple dehydrogenation steps to form *n*-C_4-dienes, while this behavior is not possible for isobutane. Thus, *n*-butane would serve both as a better reducing agent (catalyst deactivation by reduction of surface sulfate species) and as a better precursor for highly dehydrogenated hydrocarbons (catalyst deactivation by formation of carbonaceous deposits). The *n*-C_4-olefins that lead to these diene species are present in the *n*-butane feed at levels near 1000 ppm, and they may also be produced by the catalyst under reaction conditions. The longer-term deactivation is directly related to the *n*-C_4-olefins as their elimination reduced the longer-term deactivation constant for a pure *n*-butane feed by an order of magnitude. The slower deactivation observed for isobutane isomerization may be related in part to the lack of impurities in the feed capable of forming dienes, since the main olefinic impurity, isobutylene, cannot form a diene species.

CONCLUSIONS

Isomerization of *n*-butane and isobutane at 423 K over sulfated zirconia involves bimolecular reactions in which two adsorbed *n*-C_4 species react reversibly, probably through a C_8 intermediate, to form one *i*-C_4 species and in which two adsorbed *i*-C_4 species react reversibly to form one *n*-C_4 species. The rate expression based on these reactions describes not only the observed isomerization rates but also describes the measured rates of disproportionation products (i.e., C_3 and C_5 species). Further, this rate expression has been extended to describe adequately C_4 isomerization kinetics over a modified sulfated zirconia at 333 K.

The sulfated zirconia catalyst undergoes rapid initial deactivation during *n*-butane isomerization at 423 K, and the longer-term deactivation rate increases with increasing *n*-butane pressure. The rate of catalyst deactivation is slow during isobutane isomerization. We suggest that the more rapid catalyst deactivation during *n*-butane isomerization is caused by the formation of *n*-C_4-diene species from *n*-C_4 olefins that are present in the *n*-butane feed or that are produced on the catalyst under reaction conditions.

ACKNOWLEDGMENTS

This work was supported by funds provided by the Office of Basic Energy Sciences of the U.S. Department of Energy (DE-FG02-84ER13183). For providing graduate fellowships, we thank Amoco Oil Company (M.R.G.), the National Defense Science and Engineering program (K.B.F.), and the Wisconsin Alumni Research Foundation (J.M.K.). Finally, we thank the ChE 562 class (Special Topics in Chemical Engineering, Fall 1995) for their help in the collection and analysis of the kinetic data reported in this study.

REFERENCES

1. Arata, K., *Adv. Catal.* **37**, 165 (1990).
2. Adeeva, V., Lei, G. D., and Sachtler, W. M. H., *Appl. Catal. A* **118**, L11 (1994).
3. Adeeva, V., Lei, G. D., and Sachtler, W. M. H., *Catal. Lett.* **33**, 135 (1995).
4. Cheung, T. K., d'Itri, J. L., and Gates, B. C., *J. Catal.* **151**, 464 (1995).
5. Zarkalis, A. S., Hsu, C. Y., and Gates, B. C., *Catal. Lett.* **29**, 235 (1994).
6. Garin, F., Seyfried, L., Girard, P., Maire, G., Abdulsamad, A., and Sommer, J., *J. Catal.* **151**, 26 (1995).
7. Fogash, K. B., Yaluris, G., González, M. R., Ouraipryvan, P., Ward, D. A., Ko, E. I., and Dumesic, J. A., *Catal. Lett.* **32**, 241 (1995).
8. Yaluris, G., Larson, R. B., Kobe, J. M., González, M. R., Fogash, K. B., and Dumesic, J. A., *J. Catal.* **158**, 336 (1996).
9. Liu, H., Adeeva, V., Lei, G. D., and Sachtler, W. M. H., *J. Mol. Catal. A* **100**, 35 (1995).
10. Brouwer, D. M., *in* "Chemistry and Chemical Engineering of Catalytic Processes" (R. Prins and G. C. A. Schuit, Eds.), Vol. 137. Sijthoff & Noordhoff, Alphen a/d Rijn, 1980.
11. Boronat, M., Viruela, P., and Corma, A., *J. Phys. Chem.* **100**, 633 (1996).
12. Zarkalis, A. S., Hsu, C. Y., and Gates, B. C., *Catal. Lett.* **37**, 1 (1996).
13. Bearez, C., Chevalier, F., and Guisnet, M., *React. Kinet. Catal. Lett.* **22**, 405 (1983).
14. Asuquo, R. A., Eder-Mirth, G., and Lercher, J. A., *J. Catal.* **155**, 376 (1995).
15. Tábora, J. E., and Davis, R. J., *J. Catal.* in press (1996).
16. Hsu, C. Y., Heimbuch, C. R., Armes, C. T., and C, G. B., *J. Chem. Soc. Chem. Commun.*, 1645 (1992).
17. Bearez, C., Avendano, F., Chevalier, F., and Guisnet, M., *Bull. Soc. Chim. Fr.* **3**, 346 (1985).
18. Box, G. E. P., Hunter, W. G., and Hunter, J. S., "Statistics for Experimenters." Wiley, New York, 1978.
19. Bates, D. M., and Watts, D. G., "Nonlinear Regression Analysis and Its Applications." Wiley, New York, 1988.
20. Fogash, K. B., González, M. R., Kobe, J. M., and Dumesic, J. A., In preparation (1996).
21. Yori, J. C., Luy, J. C., and Parera, J. M., *Appl. Catal.* **46**, 103 (1989).
22. Ng, F. T. T., and Horvát, N., *Appl. Catal. A* **123**, L197 (1995).
23. Garin, F., Andriamasinoro, D., Abdulsamad, A., and Sommer, J., *J. Catal.* **131**, 199 (1991).
24. Comelli, R. A., Vera, C. R., and Parera, J. M., *J. Catal.* **151**, 96 (1995).
25. Chen, F. R., Courdurier, G., Joly, J., and Vedrine, J. C., *J. Catal.* **143**, 616 (1993).